energies

MDPI

Article

Extremal Dependence Modelling of Global Horizontal Irradiance with Temperature and Humidity: An Application Using South African Data

Caston Sigauke [1,†], Thakhani Ravele [1,*,†] and Lordwell Jhamba [2]

[1] Department of Mathematical and Computational Sciences, University of Venda, Private Bag X5050, Thohoyandou 0950, South Africa
[2] Department of Physics, University of Venda, Private Bag X5050, Thohoyandou 0950, South Africa
* Correspondence: ravelethakhani@gmail.com; Tel.: +27-76-664-6979
† These authors contributed equally to this work.

Abstract: The interaction between global horizontal irradiance (GHI) and temperature helps determine the maximum amount of solar power generated. As temperature increases, GHI increases up to the point that it increases at a decreasing rate and then decreases. Therefore, system operators need to know the maximum possible solar power which can be generated. Using the multivariate adaptive regression splines, extreme value theory and copula models, the present paper seeks to determine the maximum temperature that will result in the generation of the maximum GHI ceteris paribus. The paper also discusses extremal dependence modelling of GHI with temperature and relative humidity (RH) at one radiometric station using South African data from 16 November 2015 to 16 November 2021. Empirical results show that the marginal increases of GHI converge to 0.12 W/m^2 when temperature converges to 44.26 °C and the marginal increases of GHI converge to −0.1 W/m^2 when RH converges to 103.26%. Conditioning on GHI, the study found that temperature and RH variables have a negative extremal dependence on large values of GHI. Due to the nonlinearity and different structure of the dependence on GHI against temperature and RH, unlike previous literature, we use three Archimedean copula functions: Clayton, Frank and Gumbel, to model the dependence structure. The modelling approach discussed in this paper could be useful to system operators in power utilities who must optimally integrate highly intermittent renewable energies on the grid.

Keywords: archimedean copulas; bivariate threshold excess model; conditional multivariate extreme value; extreme value mixture model; global horizontal irradiance; laplace margins

Citation: Sigauke, C.; Ravele, T.; Jhamba, L. Extremal Dependence Modelling of Global Horizontal Irradiance with Temperature and Humidity: An Application Using South African Data. *Energies* **2022**, *15*, 5965. https://doi.org/10.3390/en15165965

Academic Editor: Ignacio Mauleón

Received: 13 July 2022
Accepted: 14 August 2022
Published: 17 August 2022

1. Introduction

1.1. Context

Sustainable energy supply can be achieved through renewable energy such as solar energy, which is still underused. Solar energy is environmentally friendly since there are no greenhouse emissions when electricity is generated using this resource. This reduces the effects of climate change. The challenge in using renewable energies such as solar is that they are highly intermittent [1]. Solar energy is projected to make up a significant part of the world's energy supply in the future. Accurate forecasting is needed to model intermittent solar energy spatially and temporally. Integrating renewable energy sources into the grid is likely to be one of the most significant challenges of the future world's energy supply [2]. Solar power forecasting is essential for power system operation and adds ancillary services during times of high penetration of renewable energy to avoid variability and uncertainty problems [1]. Due to the intermittence, instability and randomness, it is not easy to produce accurate, reliable forecasts of solar irradiance that can be used as a guide for operating modern smart grids for electricity generation and distribution. Global horizontal irradiance (GHI) hitting the ground surface is the same as electricity generated by photovoltaic (PV)

systems. GHI depends on the weather to produce considerable power, so understanding the weather is essential [3].

Solar power generation is primarily affected by meteorological factors such as solar radiation, temperature, humidity and wind pressure. Since GHI depends on meteorological variables, it is important to determine the extremal dependence and correlation between GHI with temperature and relative humidity. It is also important to determine the temperature value which gives us the maximum GHI. This is important as it enables us to maintain the optimal electrical power grid operation, reliability, stability and power dispatching abilities [4].

There have been some earlier studies on forecasting GHI, although most concentrate on forecasting the means or averages of the distribution. However, this study aims to model the dependence of the extreme GHI on temperature and RH. Understanding solar energy's peak power production requires analysis of GHI at the extreme tails. The weather variables, temperature and RH, which are the main drivers of GHI, are used to improve accuracy.

1.2. Literature Review

Although there are several papers which have used South African data in modelling and forecasting global horizontal irradiance (GHI), none, to the best of our knowledge, has used conditional multivariate extreme value theory together with copula functions in modelling the dependence and correlation of GHI with temperature including GHI with relative humidity. Studies focusing on short-term forecasting of GHI using data from South Africa include others [5,6]). Reference [7] provided a detailed review of the current models used to forecast solar irradiance to assist in choosing the best forecast model. The study found that the choice of best forecasting models depends on the availability of data and forecast horizon. Furthermore, the smaller the horizon, the better the accuracy [7]. To effectively manage the operations and evaluate the economic performance of power systems, it is, therefore, imperative to predict the power output of PV systems.

Multivariate Adaptive Regression Spline (MARS) models were used to assess individual parameter sensitivity. In terms of accuracy and interpretability, MARS models produced good results. The proposed MARS models are more applicable than others due to their flexibility and simplicity. The MARS model was also suggested as a feasible alternative by Li et al. [8] due to its simplicity and reasonable interpretation. MARS is a nonparametric and improved version of the traditional linear regression model that maintains the clarity of the conventional multiple linear regression. Due to its nonparametric property, the MARS model provided reliable results in training and forecasting. A related study by Li et al. [9] suggested a model for predicting hourly global solar radiation on a horizontal surface, especially for areas with restricted measured meteorological parameters using the MARS model.

The MARS method produces easily understood results by management, making it an excellent tool for handling high-dimensional problems with complex model structures, such as nonlinearity, interactions, and missing data [10]. Reference [10] developed a MARS model for predicting daily electricity peak demand. The study concluded that the MARS model outperformed the piecewise linear regression model and is easy to explain to management.

Joint tail models, copulas, and other multivariate extreme methods assume that all the variables will be large simultaneously. The conditional extremes model (CEM) overcomes this limitation [11–13]. When studying the relationship between several variables, conditional extremes modelling is crucial [14]. Reference [14] used a bivariate conditional extremes model and time-varying threshold to model the extremal dependence of monthly maximum temperature at four meteorological stations of Limpopo province, South Africa. The results showed significant positive and negative extremal dependence in some meteorological stations. Another study by [15] used the conditional extreme value modelling approach in modelling the dependence of extreme temperatures at three meteorological stations in the Limpopo province of South Africa. The authors argued that since the temper-

ature is a major driver of electricity demand, the occurrence of extremely high temperatures impacts electricity generation to meet demand.

Copulas are used in modelling the dependence and correlation between several variables based on their marginal distributions [16]. There are several types of copulas models and among them are the Archimedean, extreme value, Gaussian and Student's-*t* copulas. In this study, we focus on the Archimedean copulas. Archimedean copulas are a special type of copulas. Their properties have enabled them to be used in various areas because they are easy to construct [16]. Reference [17] fitted the Gumbel, Joe, Frank, Clayton, Gaussian and Student's-*t* copula functions to evaluate the dependence between the sky clearness index and solar radiation. Based on the Akaike Information criterion, the Gaussian copula was best used to model the extremal dependence between solar radiation and the sky clearness index. In [18] a copula-based model was used to study the relationship between the beam radiation and diffuse radiation at different locations using data from Sweden.

Another study by [19] used five copula functions to model the dependence structure of sunshine duration hours with solar radiation at nine radiometric stations in Iran. Based on the two information criteria, Akaike Information Criterion (AIC) and Schwartz information criterion, the Clayton copula yielded the best performance.

Some studies have been carried out to correlate temperature with global solar radiation. These include a study by [20] who estimated the correlation between global solar irradiation and temperature. The proposed method was applied to eight radiometric stations in Asturias, a region northwest of Spain. It was noted from the study that the results from the proposed method were able to explicitly show the influence of the distance to sea, altitude and a reference temperature. In a related study [18] used a two-variable-bivariate-copula-based approach in describing the dependency between the beam and diffuse irradiance data. It was noted from the study that the developed modelling framework significantly simplifies calculations for solar engineering applications.

To the best of the authors' knowledge, none have used MARS models, conditional multivariate extreme value models and Archimedean copulas such as Clayton, Frank and Gumbel to model the extreme dependency of GHI with temperature and RH using South African data before this study. This is the gap that this paper seeks to cover. A summary of previous studies on the modelling extremal dependence of GHI with some weather variables is given in Table 1.

Table 1. Summary of previous studies on extremal dependence modelling of GHI with temperature.

Ref.	Data	Models	Main Findings
[8]	solar power data	Extremal dependence and correlation approaches	Results show that the measures of contagion are not highly correlated
[15]	Maximum daily temperature	Bivariate threshold excess model	The results may be important to power utility companies facing uncertainty in electricity demand due to extreme temperatures.
[14]	Monthly maximum temperature	Bivariate time varying threshold excess approach	Results of the study showed some significant positive and negative extremal dependence in some pairs of meteorological stations
[19]	Mean monthly solar radiation and sunshine duration hours	Bivariate parametric copula functions: elliptical (normal and Student's), Archimedean (Clayton, Frank and Gumbel)	The Clayton copula yielded the best performance.
[17]	Clearness index and solar radiation	Copula functions used were the Gumbel, Joe, Frank, Clayton, Gaussian and Student's t copulas.	The results indicated that the Gaussian copula gave the best fit to the tails of the distributions of the solar radiation and sky clearness index.
[18]	Beam and diffuse irradiance data	Two-variable-bivariate-copula	Results suggest that the modelling framework significantly simplifies calculations for solar engineering applications.

1.3. Research Highlights

This study uses South African data to address extremal dependence modelling of GHI with temperature and relative humidity (RH) at one radiometric station. The multivariate

adaptive regression spline (MARS) model is essential to model the impact of weather variables such as temperature and RH on the GHI power production. Conditional extremes modelling is important in this study to model dependence structure among temperature and RH variables on GHI. Conditioning on GHI, the study found that temperature and RH variables have a negative extremal dependence on large values of GHI. The dependence structure of GHI against temperature and RH was examined using the Archimedean copula functions such as Clayton, Frank, and Gumbel. The Frank copula was the better fit for GHI against temperature. For GHI against RH, only the Frank copula adequately fits the data. The main contribution of this study is on extremal dependence modelling of GHI with temperature and RH using South African data.

The study is divided into four sections: Section 2 presents the proposed models. Results and discussion of the empirical research were presented in Section 3, while the study's conclusion was presented in Section 5.

2. Methodology

2.1. Multivariate Adaptive Regression Spline

The multivariate adaptive regression spline (MARS) model is a nonparametric multivariate regression method developed by Friedman [21], which allows a flexible regression analysis for high-dimensional data. The general MARS model is defined by [21]:

$$f(x) = \beta_0 + \sum_{m=1}^{M} \beta_m B_m(x), \tag{1}$$

where

$$B_m(x) = \prod_{k=1}^{K_m} \left[s_{km} \left(x_{v(k,m)} - t_{km} \right) \right],$$

denotes a basis function, β_0 and β_m are parameters, M represents the number of basis functions, K_m is the number of knots, s_{km} is either 1 or -1, depending on the associated step function of right or left sense, $v(k,m)$ is the label of the independent variable and t_{km} denotes the knot location. The GCV criterion considers residual error and model complexity as a measure of goodness of fit. The GCV criterion is given by [22]:

$$\mathrm{GCV}(M) = \frac{\frac{1}{N}\sum_{i=1}^{N} \left[y_i - \hat{f}_M(x_i) \right]^2}{\left[1 - \frac{C(M)}{N} \right]^2}, \tag{2}$$

where N represents the sample size, $C(M)$ is a measure of the cost-penalty associated with a model containing M basis functions, $\hat{f}_M(x_i)$ measures the lack of fit on the basis function model of M and $C(M)$ is the penalty for model complexity in the denominator. The model with the lowest GCV criterion value is the best. The MARS model used in this study is for modelling the effect of temperature and RH on GHI. The models are given as:

$$\mathrm{GHI} = \beta_0 + \beta_1 \max(0, t_s - \mathrm{T}_t) + \beta_2 \max(0, \mathrm{T}_t - t_w) + \varepsilon_t, \tag{3}$$

$$\mathrm{GHI} = \beta_0 + \beta_1 \max(0, rh_s - \mathrm{RH}_t) + \beta_2 \max(0, \mathrm{RH}_t - rh_w) + \varepsilon_t, \tag{4}$$

where $\beta_i, i = 1, 2$ are parameters to be estimated, t_s and t_w, and rh_s and rh_w are reference temperatures and RHs which will be determined using the MARS algorithm and error term ε_t [10]. In the modelling, marginal GHI increases are estimated for each unit increase in temperature and RH above t_s and rh_s.

2.2. Conditional Multivariate Extreme Value Modelling

Joint tail models, copulas, and other multivariate extreme methods assume that all the variables will be large simultaneously. The conditional extremes model (CEM) overcomes this limitation [11–13]. Using a CEM, the dependence structure among variables is estimated where one variable is conditioned on being extreme and attempt to model the conditional distribution [11,12]. This study uses the conditional multivariate approach [11].

2.2.1. Threshold Selection

In GPD, we are interested in the observations above a sufficiently high threshold. The threshold selection is comparable to the block size selection in the block maxima method and there must be a balance between bias and variance [23]. This study will use extremal mixture models. The advantage of using extreme value mixture models is that they simultaneously capture both the bulk distribution below the threshold and the tail distribution above the threshold [24,25].

2.2.2. Bivariate Threshold Excess Model

Extreme value theory (EVT) focuses not only on modelling maxima or minima data. It also focuses on predicting the observations which are above a high threshold. The multivariate modelling in this study is limited to pairwise combinations of variables. GPD is a model used in EVT for exceedances above a threshold and is defined by [23]:

$$G(x) = 1 - \eta \left[1 + \xi \left(\frac{x-u}{\sigma_u}\right)\right]^{-\frac{1}{\xi}}, \ \xi \neq 0, \tag{5}$$

where $\eta = \Pr(X > u)$ for a family represented on $\left[1 + \xi \left(\frac{x-u}{\sigma_u}\right)\right] > 0$ and $x - u > 0$. Therefore, $F(x) \approx G(x)$ on $x > u$ for a sufficiently high threshold u with parameters η, ξ and σ_u [23]. The objective is to derive a family that approximates a joint distribution $F(x, y)$ on regions $x > u_{x,y} > u_y$ for sufficient large thresholds u_x and u_y.

2.2.3. Marginal Transformation: Laplace Margins

The margins are first transformed into standardised Laplace margins in the regression type dependence model before dependence models are built. There are symmetric and exponential tails in the Laplace distribution. Laplace margins simplify the regression structure compared to other transformations, such as Fréchet and Gumbel margins [11,12]. Therefore, both positive and negative dependence can be described by a single model structure [14]. Let

$$Y_i = \begin{cases} \log\{2F_i(X_i)\}, & \text{for } X_i < F_i^{-1}(0.5) \\ -\log\{2[1 - F_i(X_i)]\}, & \text{for } X_i > F_i^{-1}(0.5) \end{cases} \tag{6}$$

for $i \in D = \{1, 2, \ldots, d\}$. The vector $\mathbf{Y} = (Y_1, \ldots, Y_d)$ is then said to have a Laplace distribution given by [12]:

$$P(Y_i < y) = \begin{cases} e^{\frac{y}{2}}, & \text{if } y < 0 \\ 1 - e^{-\frac{y}{2}}, & \text{if } y \geq 0, \end{cases} \tag{7}$$

for all $i \in D$.

2.3. Bivariate Dependence Modelling Using Copulas

A copula approach allows us to model different types of relationships across a wide range of behaviour. In analysing the dependence structure, the copula function renders many advantages. First, copulas allow modelling marginal behaviour and dependency structures separately. Second, the copula function can show the dependence's degree and structure. In this way, asymmetric dependence can be captured since a linear correlation

does not provide information about tail dependence. Thirdly, copulas do not imply elliptically distributed random variables, unlike correlation [26]. There are different types of copulas such as the Archimedean, extreme value and elliptical copulas. This study will use Archimedean copulas due to their advantage in capturing dependencies in the upper and lower tails.

2.3.1. Sklar's Theorem

Sklar's theorem is considered the central theorem of copula theory, whereby the *n*-dimensional distribution function can be divided into two basic components, the marginal distribution and the copula [16].

Theorem 1. ***Sklar's theorem:*** *Let H denote an n-dimensional distribution function with marginals F1, F2, …, Fn. Then for all* $x_1, x_2, \ldots, x_n \in \mathbb{R}$*, there is an n-copula C,*

$$H(x_1, x_2, \ldots, x_n) = C\big(F_1(x_1), F_2(x_2), \ldots, F_n(x_n)\big). \tag{8}$$

The corresponding theorem in two dimensions is derived for $n = 2$. This important theorem shows that copula functions are essential for multivariate distribution functions whose marginals are either known or given. Based on Sklar's theorem, there is a copula C:$[0, 1]^n \rightarrow [0, 1]$. It maps the multivariate marginal distribution F_i to the univariate distribution function F. The multivariate joint density function is defined by [27]:

$$f(x_1, \ldots, x_n) = c(F_1(x_1), \ldots, F_n(x_n)) \times f_1(x_1) \times \ldots \times f_n(x_n). \tag{9}$$

2.3.2. Archimedean Copulas

Archimedean copulas are a special type of copulas. Their properties have enabled them to be used in various areas because they are easy to construct [16]. Compared to traditional techniques, Archimedean copulas are designed to produce a significantly better dependency model because they are more tractable mathematically. In addition, they can construct multivariate copulas using a simple hierarchical method, which is often ineffective with other copula classes [28]. Archimedean copulas contain dependence models that are viable for modelling upper and lower tail dependences. The Archimedean copula equation is given by [26]:

$$C_{arch}(u_1, u_2) = \Phi^{-1}\big(\Phi(u_1) + \Phi(u_2)\big), \tag{10}$$

where Φ denotes a generator function of the copula, if for all $0 \leq u_1, u_2 \leq 1$.

Numerous families present different dependency structures within the Archimedean copula, simplifying the construction of bivariate distributions [26]. This study employs three Archimedean copula functions: Clayton, Frank and Gumbel.

The Clayton Copula

Clayton copula was proposed by [29] and is given in Equation (11).

$$C_\theta^{Clayton}(u_1, u_2) = (u_1^{-\theta} + u_2^{-\theta} - 1)^{-\frac{1}{\theta}}, \tag{11}$$

where $\theta \in [-1, \infty)/\{0\}$ controls the degree of dependence between u_1 and u_2. The bivariate Clayton copula function converges to the comonotonic copula if $\theta = 0$ and tail independence if $\theta \rightarrow 0$. If $\theta = -1$, we obtain the lower bound of Fréchet-Hoeffding. Kendall's tau is defined as the bivariate Clayton copula function parameter as follows:

$$\tau_k = \frac{\theta}{\theta + 2}. \tag{12}$$

The lower tail dependence is estimated using the following function:

$$\lambda^L = 2^{-\theta}. \tag{13}$$

The Frank Copula

Frank copula was proposed by [30] and is given in Equation (14).

$$C_{\theta}^{Frank}(u_1, u_2) = -\frac{1}{\theta}\ln\left(1 + \frac{(e^{-\theta u_1} - 1)(e^{-\theta u_2} - 1)}{(e^{-\theta} - 1)}\right), \tag{14}$$

where θ is any real number. Based on the dependence parameter (θ), the upper and lower Fréchet-Hoeffding bounds can be estimated. The model is not tail dependent ($\lambda_{u_1} = \lambda_L = 0$) and is suitable for modelling data with weak tail dependency.

The Gumbel Copula

Gumbel copula was proposed by [31] and is given in Equation (15).

$$C_{\theta}^{Gumbel}(u_1, u_2) = \exp\left(-\left[(-\ln u_1)^{\theta} + (-\ln u_2)^{\theta}\right]^{\frac{1}{\theta}}\right); \qquad 0 \leq u_1, u_2 \leq 1, \tag{15}$$

where $\theta \in [1, \infty)$ determines the degree of dependence between u_1 and u_2. When $\theta = 1$, the bivariate Gumbel copula converges to complete independence, and when $\theta \to 0$, perfect independence is achieved. Kendall's tau (τ) and the bivariate Gumbel parameter (θ) are linked by the following formula:

$$\tau_k = 1 + \theta^{-1}. \tag{16}$$

To estimate the upper (λ^U) and lower (λ^L) tail dependence of the bivariate Gumbel copula, the following functions are used:

$$\lambda^U = 1 + 2^{-\theta} \text{ and } \lambda^L = 0.$$

2.3.3. The Bivariate Archimedean Copula Parameter (θ) and Its Relationship with the Kendall's Tau (τ) and Tail Dependence (λ^U and λ^L)

As discussed in [26], Archimedean copula functions are attractive due to their relationship with the tail dependence coefficient and Kendall's tau. Table 2 presents the relationship between bivariate Archimedean copula parameters (θ), tail dependence coefficients: Kendall's tau (τ) and tail dependence (λ^U and λ^L). The Clayton copula is an asymmetric copula that exhibits lower tail dependence. The Gumbel copula function represents the upper tail dependence, which is also an asymmetric copula. This indicates that the compound variables are moving upwards rather than downwards at the same time. The tail dependence coefficient (λ^U and λ^L) is a measure of how dependent two variables are on each other's tails.

Table 2. The relationship between the bivariate Archimedean copula parameter (θ) and tail dependence coefficients: Kendall's tau (τ) and tail dependence (λ^U and λ^L).

Family	Copula Parameter (Θ)	Kendal's Tau (τ)	Upper Tail (λ^U)	Lower Tail (λ^L)
Clayton	$\theta > 1$	$\frac{\theta}{\theta+2}$	0	$2^{-\theta}$
Frank	$-\infty < \theta < \infty$	$1 - \frac{4}{\theta}[D_j(\theta)]$	0	0
Gumbel	$\theta \geq 1$	$\frac{\theta-1}{\theta}$	$2 - 2^{-\theta}$	0

2.3.4. Parameter Estimation and Goodness of Fit Tests

The Archimedean copula functions in this study have only one dependence parameter, which will be estimated using the maximum likelihood method. The Akaike Information Criterion (AIC) and Bayesian Information Criterion (BIC) will be used to select the best fitting Archimedean copula models. The AIC and BIC are given by:

$$\text{AIC} = 2\ell + 2k, \tag{17}$$

and

$$\text{BIC} = 2\ell + \ln(n)k, \tag{18}$$

where ℓ represents the log-likelihood and ln the natural logarithm.

2.3.5. Mixture of Copulas

Let $C_i(u_1, u_2)$ denote a copula i, $i = 1, \ldots, m$, i.e., m copulas of dimension d. A mixture of these $d-$dimensional copulas with weights w_i, $i = 1, \ldots, m$ is also a $d-$dimensional copula whose distribution function is given by Equation (19).

$$C^{\text{mix}}(u_1, u_2) = \sum_{i=1}^{m} w_i C_i(u_1, u_2), \tag{19}$$

with $\sum_{i=1}^{m} w_i = 1$, i.e., the mixture is a convex combination of the m copulas.

3. Empirical Results

The hourly GHI data used in this study are from Southern African Universities Radiometric Network (SAURAN) website (https://sauran.ac.za/, accessed on 27 November 2021) from 16 November 2015 to 16 November 2021, giving a sample size of n = 27,274 observations. The University of Venda radiometric station was chosen for this study. It is located at the Vuwani Science Research Centre in Limpopo, South Africa, at latitude −23.13100052, longitude 30.42399979 and an elevation of 628 m. The R software was used for all the statistical analysis that was undertaken in this paper.

3.1. Exploratory Data Analysis

A summary of hourly GHI statistics is presented in Table 3. The distribution of GHI data does not resemble a normal distribution since the mean and median are not equal. Skewness and kurtosis values of 0.5109 and −0.9320, respectively, confirm the non-normality of the distribution of GHI data. The skewness and kurtosis values in Table 3 indicate that the temperature and relative humidity (RH) distributions are non-normal. The distribution of temperature data is skewed to the right and the kurtosis value shows that the distribution is platykurtic. However, the distribution of RH data is skewed to the left and kurtosis is platykurtic.

Figure 1 displays hourly GHI superimposed. The non-linear trend was estimated based on the generalised additive model discussed in [32].

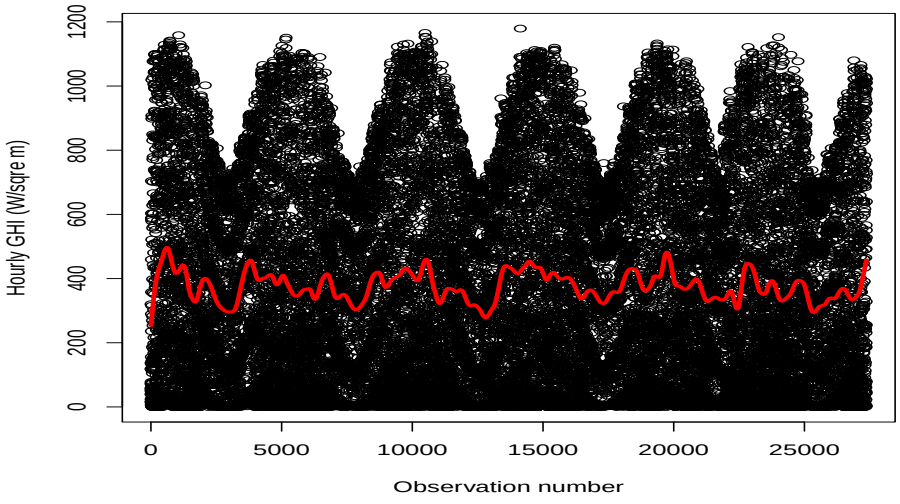

Figure 1. Plot of hourly GHI from 16 November 2015 to 16 November 2021 superimposed with a non-linear trend.

Table 3. Summary statistics for GHI, temperature and RH.

Variable	Mean	Median	Mini	Maxi	Std	Skewness	Kurtosis
GHI	375.642	312.041	0.100	1179.16	314.736	0.511	−0.932
Temp	24.5 °C	24.2 °C	4.9 °C	43.2 °C	5.9 °C	0.1 °C	−0.4 °C
RH	58.365%	57.810%	5.428%	100%	22.607%	−0.015%	−0.962%

3.2. Results for Estimating Extreme Quantiles

3.2.1. MARS Models

Temperature against GHI

The R statistical package "earth" developed by [33] was used to estimate the reference temperatures, t_s and t_w in Equation (3). Knots were estimated at t_s = 19 °C and t_w = 30 °C. System operators need an analysis of the effects of high temperatures above 30 °C to design, operate and maintain their power plants. By estimating the parameters and knots of the MARS model for GHI against Temperature, we obtained:

$$\hat{\text{GHI}} = 420 + 24 * \max(0, \text{T}_t - 19) - 17 * \max(0, 30 - T_t) - 18 * \max(0, T_t - 30) \quad (20)$$

The top panel of Figure 2 shows how GHI and temperature superimposed with the estimated MARS model in Equation (20) are related. Equation (21) presents a summary of the piecewise linear functions, which the MARS model estimated.

$$\hat{\text{GHI}} = \begin{cases} \hat{\text{GHI}} = 420 - 17 * \max(0, 30 - T_t), & \text{if } T_t < 19\ ^\circ\text{C} \\ \hat{\text{GHI}} = 420 + 24 * \max(0, T_t - 19) - 17 * \max(0, 30 - T_t), & \text{if } 19\ ^\circ\text{C} \leq T_t \leq 30\ ^\circ\text{C} \\ \hat{\text{GHI}} = 420 + 24 * \max(0, T_t - 19) - 18 * \max(0, T_t - 30), & \text{if } T_t > 30\ ^\circ\text{C} \end{cases} \quad (21)$$

We then estimated the gradients of the piecewise linear functions given in Equation (21). The gradient of the linear model for which $T_t < 19$ °C was found to 17, for 19 °C $\leq T \leq$ 30 °C the gradient was estimated as 41 and for $T_t > 30$ °C it was 24. This means for 19 °C $\leq T \leq$ 30 °C for a one-degree increase in temperature; there will be an increase of 41 MW.

RH against GHI

The knots of RH were estimated using the MARS model for GHI against RH. They were estimated as $\hat{rh}_s$ = 48% and $\hat{rh}_w$ = 84%. By estimating the parameters and knots of the MARS model for GHI against RH, we obtained:

$$\hat{\text{GHI}} = 540 + 1.1 * \max(0, 48 - \text{RH}_t) - 12 * \max(0, \text{RH}_t - 48) + 6.8 * \max(0, \text{RH}_t - 84) \quad (22)$$

Equation (23) presents a summary of the piecewise linear functions estimated by the MARS model for the GHI and RH data.

$$\hat{\text{GHI}} = \begin{cases} \hat{\text{GHI}} = 540 + 1.1 * \max(0, 48 - \text{RH}_t), & \text{if } \text{RH}_t < 48 \\ \hat{\text{GHI}} = 540 - 12 * \max(0, \text{RH}_t - 48), & \text{if } 48 \leq \text{RH}_t \leq 84 \\ \hat{\text{GHI}} = 540 - 12 * \max(0, \text{RH}_t - 48) + 6.8 * \max(0, \text{RH}_t - 84), & \text{if } \text{RH}_t > 84 \end{cases} \quad (23)$$

Figure 2 bottom panel shows how GHI and RH are superimposed with the estimated MARS model in Equation (22). The estimated gradients for the piecewise linear functions are as follows: For $\text{RH}_t < 48$, we obtain −1.1; for $48 \leq \text{RH}_t \leq 84$ we obtain −12 and for $\text{RH}_t > 84$, the estimated gradient was found to be −5.

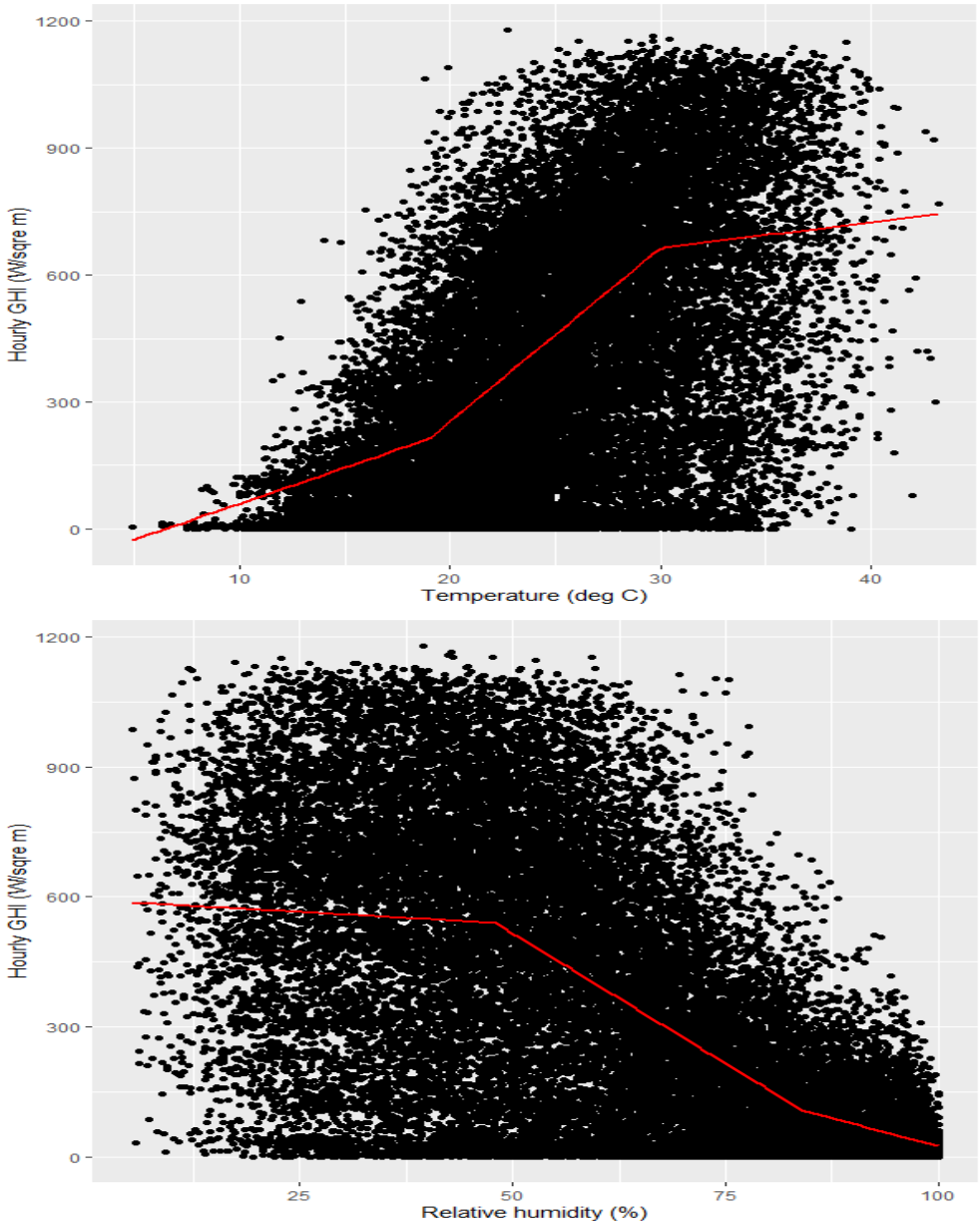

Figure 2. (**Top panel**): Plot of GHI versus Temperature. (**Bottom panel**): Plot of Relative humidity versus GHI.

3.2.2. Threshold Estimation

The R package 'evmix' developed by [34] is used to estimate thresholds as shown in Figure 3 top and bottom panels, respectively. This is based on the extremal models discussed in Section 2.2.1. Figure 3 top panel shows a temperature density function of the parametric extreme value mixture model with Weibull distribution for bulk and the tails of the GPD, with bulk and parameterised tail fraction approach, where the vertical lines indicate the thresholds. The thresholds at which the tail fraction would be considered sufficiently high are 32.4 °C and 30.96 °C for bulk and parameterised tail fraction, respectively. Figure 3 bottom panel shows an RH density function of the parametric extreme value mixture model with Weibull distribution for bulk and the tails of the GPD, with bulk and parameterised tail fraction approach. The thresholds at which the tail fraction would be considered sufficiently high are 90.2% for bulk tail fraction and 89.9% parameterised tail fraction. In Figures A2 and A3 given in the appendix, the marginal diagnostic plots for temperature show that the points are linear, suggesting that the parameterised tail fraction fits the data

well. Figures A4 and A5 given in the appendix illustrate marginal diagnostic plots of the RH data, which indicate a good fit of the parameterised tail fraction.

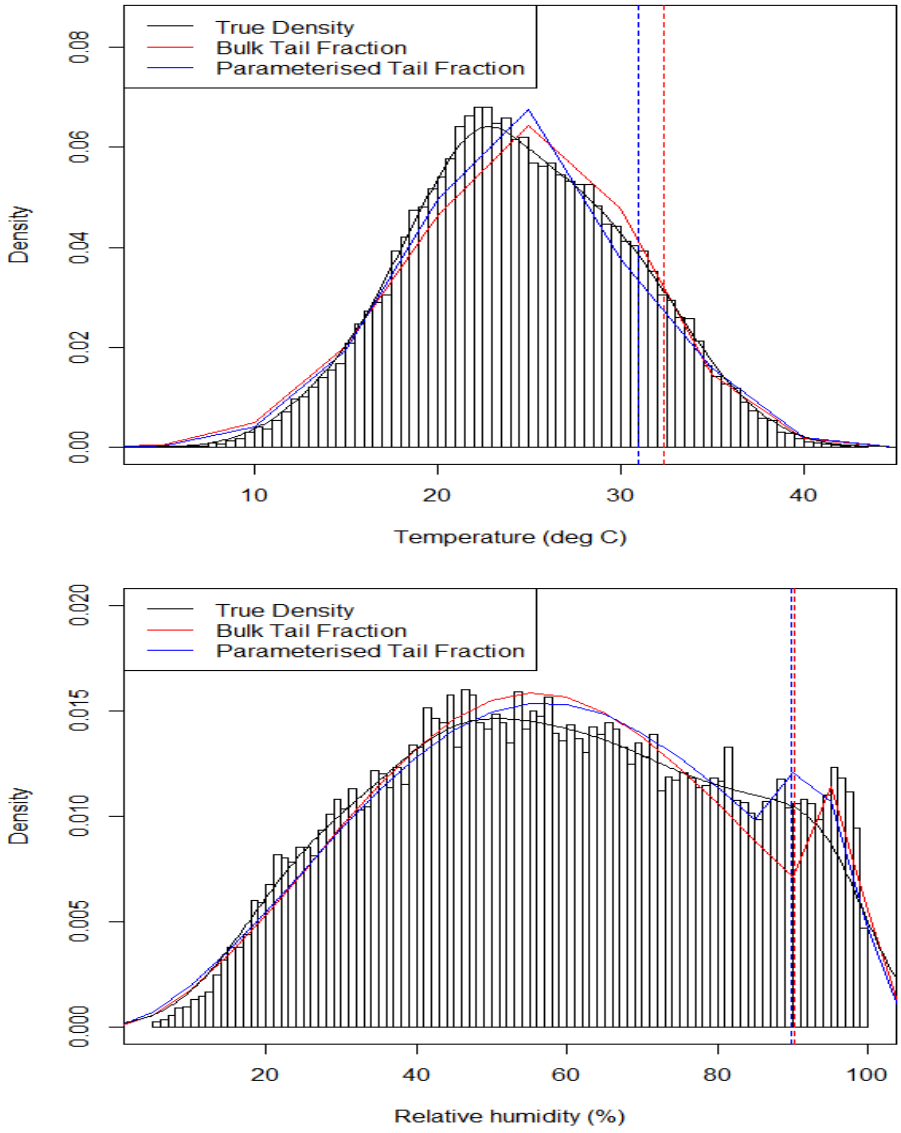

Figure 3. Top panel: Density function of temperature. **Bottom panel:** Density function of relative humidity.

3.2.3. Quantile Estimation for Marginal Increases

Table 4a shows estimated quantiles based on various tail probabilities and marginal increases in GHI against Temperature. The marginal increase of the GHI converges to 0.12 W/m^2 as the temperature converges to 44.26 °C over the sampling period of 16 November 2015 to 16 November 2021. This analysis is crucial for system operators in scheduling and dispatching electrical power. In Table 4b, the marginal increase of the GHI converges to -0.1 W/m^2 as the RH converges to 103.26% over the sampling period of 16 November 2015 to 16 November 2021. The marginal increases of the GHI with Temperature and RH are also shown in Figure 4 top and bottom panels, respectively.

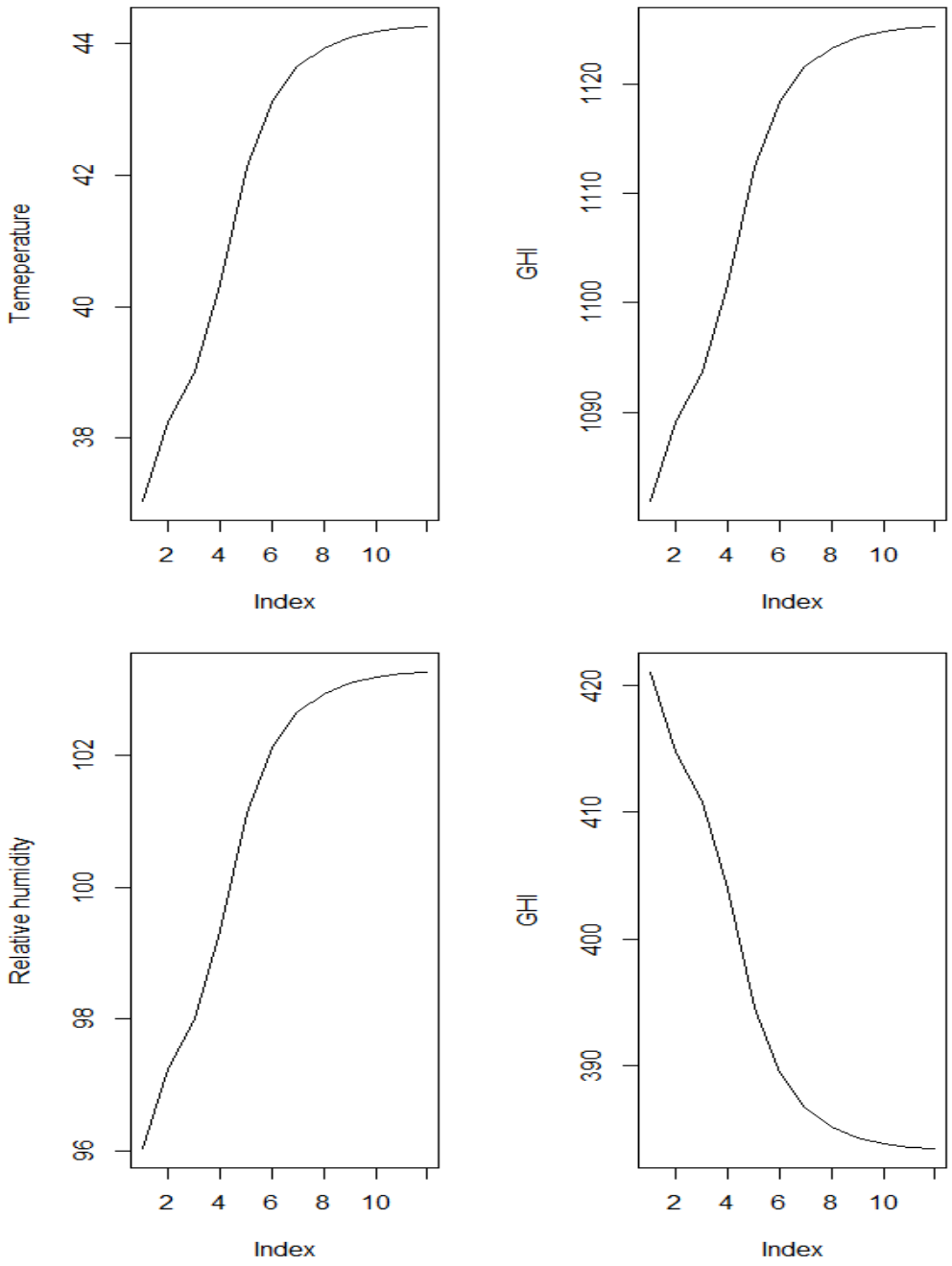

Figure 4. (**Top panel**): Plots for quantile estimation of temperature. (**Bottom panel**): Plots for quantile estimation of RH.

Table 4. (**a**) Estimated quantiles at different tail probabilities and marginal increases in GHI against Temperature. (**b**) Estimated quantiles at different tail probabilities and marginal increases in GHI against RH.

(a)			
Quantile	**GHI (W/m^2)**	**Temperature (x_p)**	**Marginal Increase in GHI (W/m^2)**
90th	1081.88	37.04	
95th	1089.08	38.24	7.2
97th	1093.70	39.01	4.62
99th	1101.62	40.33	7.92
99.9th	1112.42	42.13	10.8
99.99th	1118.30	43.11	5.88
99.999th	1121.54	43.65	3.24
99.9999th	1123.28	43.94	1.74
99.99999th	1124.24	44.10	1.5
99.999999th	1124.78	44.19	0.54
99.9999999th	1125.08	44.24	0.3
99.99999999th	1125.20	44.26	0.12
(b)			
Quantile	**GHI (W/m^2)**	**RH (x_p)**	**Marginal Increase in GHI (W/m^2)**
90th	421.03	96.04	
95th	414.79	97.24	−6.24
97th	410.79	98.01	−4
99th	403.92	99.33	−6.87
99.9th	394.56	101.13	−9.36
99.99th	389.47	102.11	−5.09
99.999th	386.66	102.65	−2.81
99.9999th	385.15	102.94	−1.51
99.99999th	384.32	103.10	−0.83
99.999999th	383.85	103.19	−0.47
99.9999999th	383.59	103.24	−0.26
99.99999999th	383.49	103.26	−0.1

3.2.4. Parameter Estimates of the Bivariate Threshold Excess Models

In Figure 5 for GHI, the marginal diagnostic plots show that the points are linear, suggesting that the model fits the data well.

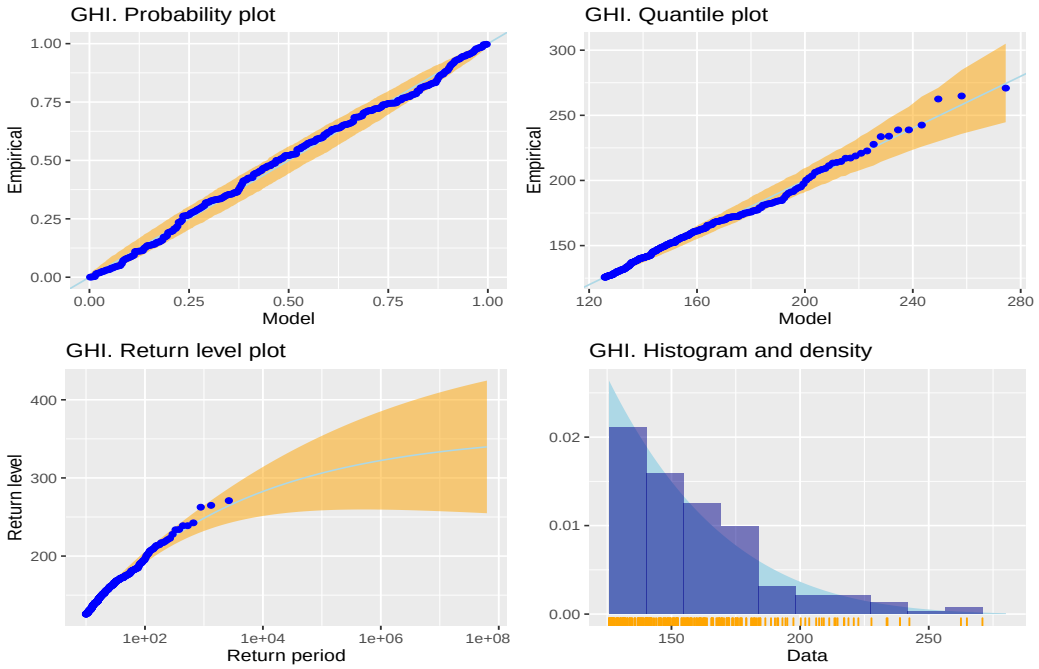

Figure 5. Marginal diagnostic plots for GHI.

Multivariate conditional Spearman's ρ correlation plots are shown in Figure 6, where ρ is Spearman's coefficient of correlation. Figure 6 shows a very weak and positive correlation between temperature and GHI, whereas RH and GHI are negatively correlated.

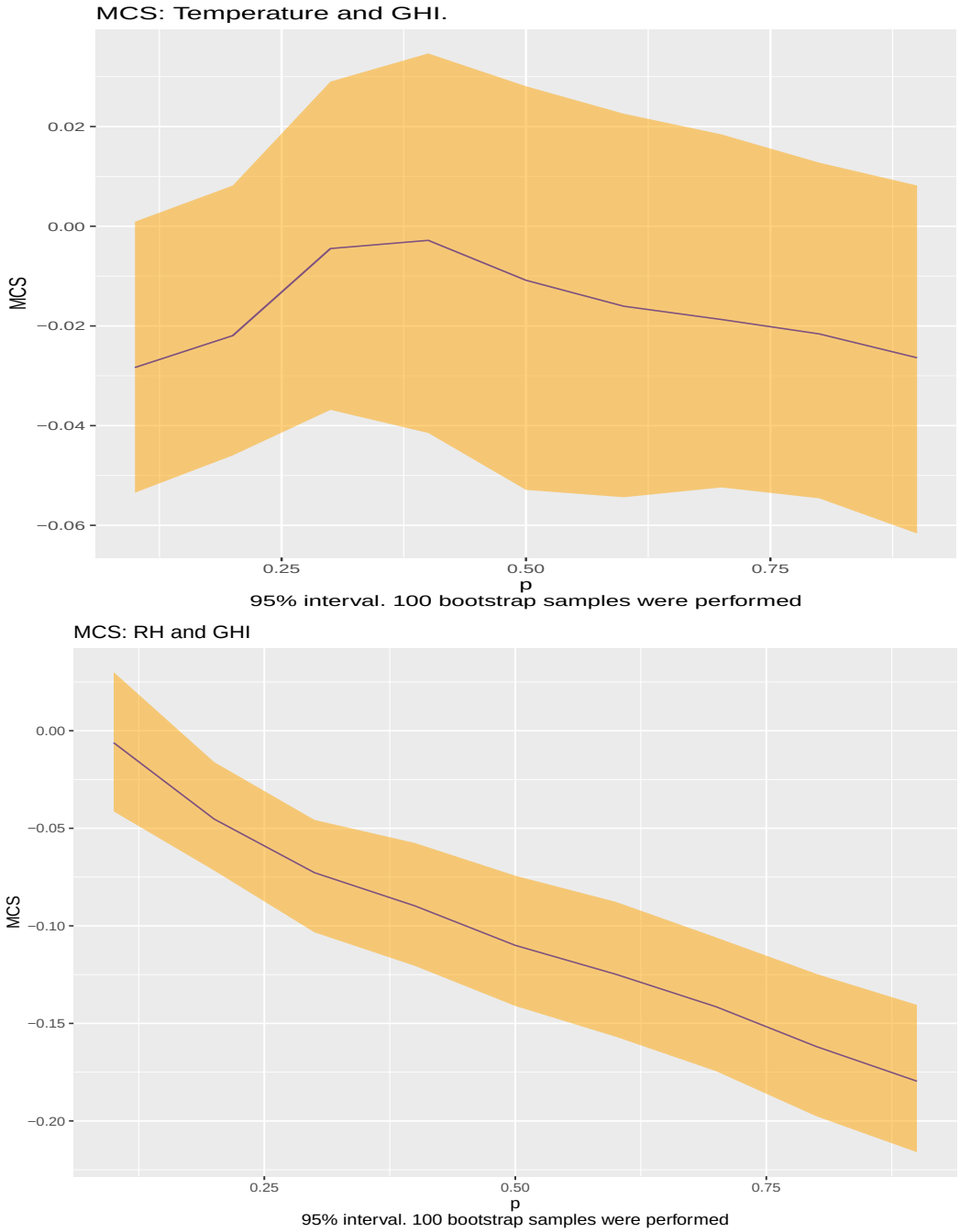

Figure 6. MCS plots with associated 95% bootstrap confidence intervals.

The structure of the dependence model is simplified by Laplace margins presented in Section 2.2.3. As a result, a single structure can be used to describe both positive and negative dependence [11]. A constrained Laplace margin for dependence estimation determines the threshold quantile of the transformed data as $\tau = 0.9$. Marginal quantiles defined by the threshold will be used in fitting the marginal GPD models in this study. In this study, marginal models and dependence models are used for modelling. This study focuses primarily on modelling extremal dependence modelling of GHI on temperature and RH. Table 5 presents estimates of a and b, which are the target parameters of the dependence structure models. According to [11], there is a strong negative and positive extremal dependence for the estimates of the parameter a close to -1 and 1. Conditioning on GHI, the estimates of the dependence parameters for temperature and RH variables are

$a = -0.1187$ and $a = -0.2183$, respectively. This suggests that temperature and RH variables have a negative extremal dependence on large values of GHI.

Figure 7 shows the diagnostic plots for conditioning GHI on temperature and RH. From top to bottom, the plots show dependence model residuals across the range of the extreme conditioning variable, the absolute values of the centred and scaled values of the residuals across the range of the extreme conditioning variable and the original untransformed data with contours showing quantiles of the fitted conditional model. The horizontal lines in Figure 7 are smoothest at the 90th percentile, where the parameter estimates are stable. The diagnostic plots displayed the same characteristics for conditioning GHI on temperature and RH.

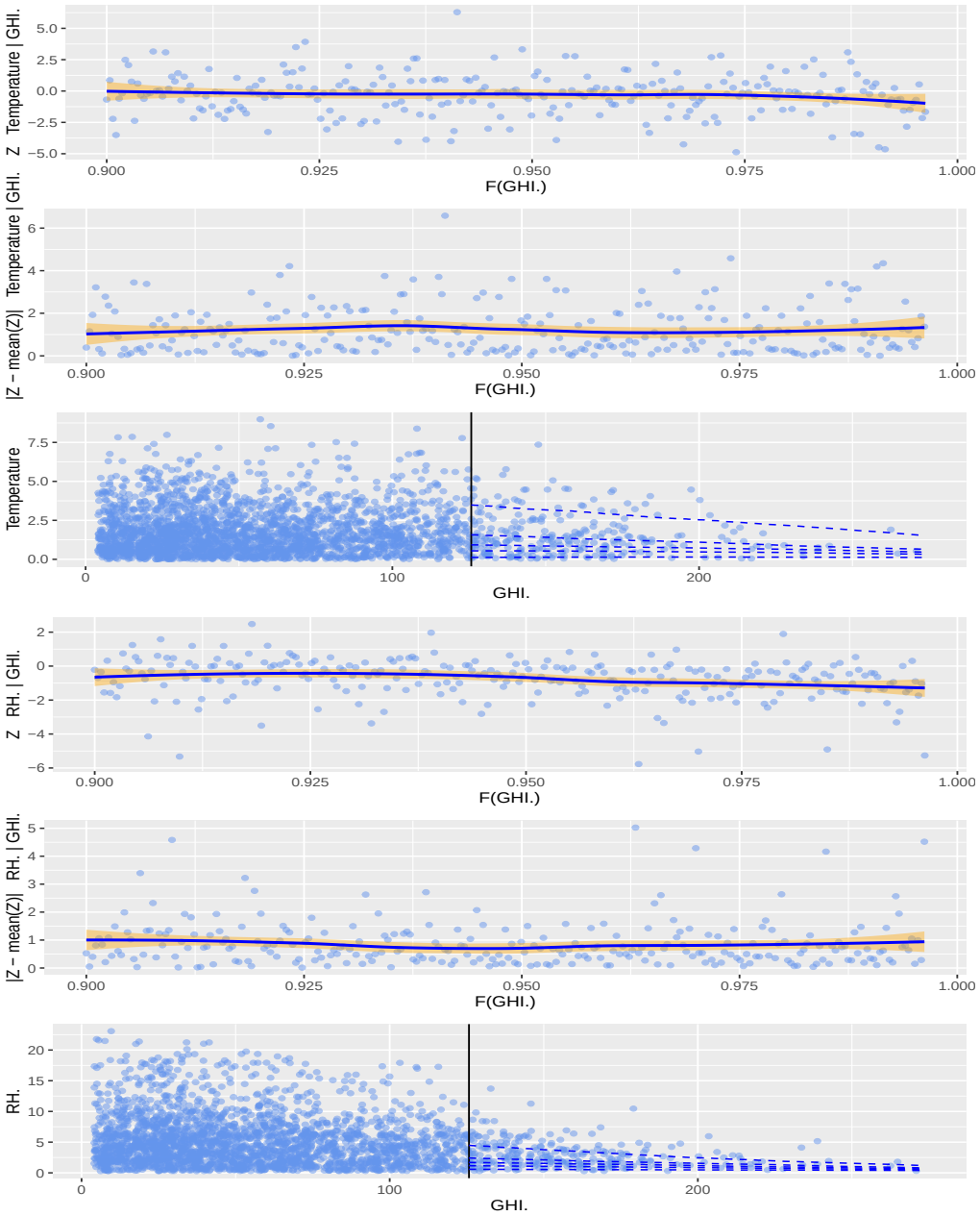

Figure 7. Diagnostic plots for conditioning GHI on Temperature and RH.

Table 5. Estimates of dependence models.

	Dependence Parameters	Temperature	RH
Conditioning on GHI	a	−0.1187 *	−0.2183 *
	b	−0.2774	−0.1236

* denotes significant positive or negative values at 5% significance level.

3.2.5. Fitting Archimedean Copulas

Table 6 shows the estimates of bivariate Archimedean copula function parameters of the GHI against temperature and RH and the dependence structure. The estimated copula function parameters are positive for GHI against temperature. This indicates an upper tail dependence. Based on log-likelihood, AIC and BIC, the Frank copula gives better fits because of the highest value of log-likelihood and lowest value of AIC and BIC. The Frank copula is the only one that fits the data well for GHI against RH. The Clayton copula does not fit the data well. For the Frank copula, both upper and lower tail dependencies are zero, which means weak lower and upper tail dependencies. The parameter estimate in Table 6b for the Gumbel copula is 1, showing that it is at the boundary suggesting independence. As a result, a Gumbel copula is not a good fit. These results have important implications for power demand risk management.

Table 6. (**a**) Parameter estimation for the Archimedean copula functions of GHI against temperature. (**b**) Parameter estimation for the Archimedean copula functions of GHI against RH.

(a)

Copula	Estimate	ℓ	AIC	BIC	λ^U	λ^L	τ
Clayton	1.3157	1717	−3431.474	−3423.256	0	0.6114	0.2619
Frank	4.04	5086	−10169.42	−10161.2	0	0	0.3911
Gumbel	1.5099	4175	−8348.908	−8340.691	1.6489	0	0.3377

(b)

Copula	Estimate	ℓ	AIC	BIC	λ^U	λ^L	τ
Clayton	0.02509	−255	512	520	0.9827593	0	0.0124
Frank	−4.0986	5232	−10461.06	−10452.84	0	0	−0.3954
Gumbel	1	−0.0003	2.0007	10.218	1.5	0	0

The contour plots of the Archimedean copula functions are shown in Figure 8. As can be observed from the figures, the estimated Frank and Gumbel copulas for GHI against temperature are characterised by lower and upper tails dependence. Only the lower tail dependence characterises the estimated Clayton copula. The contour plots show that the Clayton and Gumbel copula for GHI against RH cannot fit the data effectively.

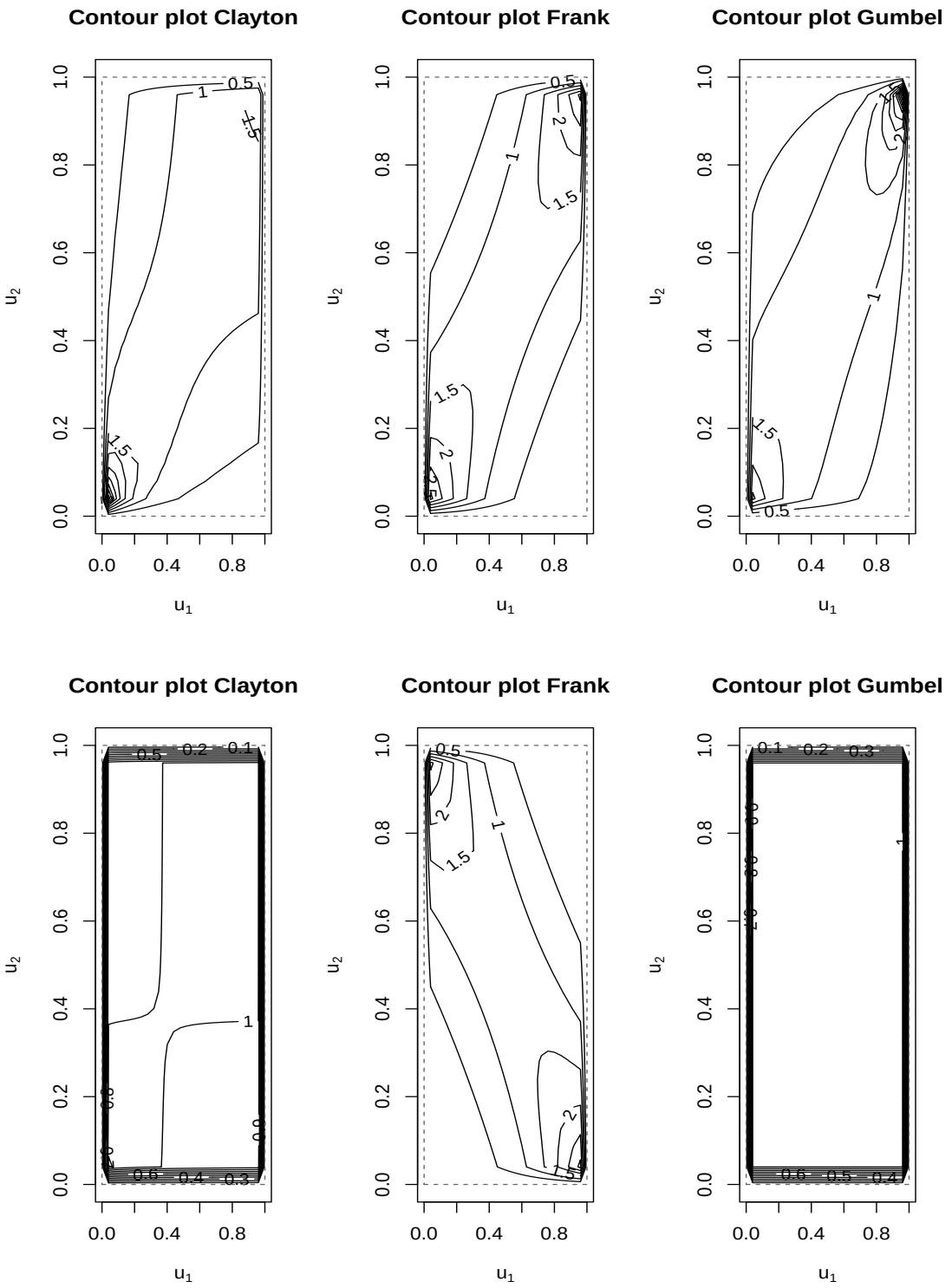

Figure 8. Top panel: Contour plots of the joint distribution for the Frank, Clayton and Gumbel for GHI against temp. **bottom panel:** Contour plots of the joint distribution for the Frank, Clayton and Gumbel for GHI against RH.

3.2.6. Mixture of Archimedean Copulas

The Frank and Gumbel copulas are used to create the mixture copula because they are the better fit for GHI against temperature from Table 6 and Figure 8 top panel. The Frank-Gumbel copula also gives a good fit to the GHI-temperature data. From Equation (19) we have

$$\begin{aligned} C_{FG}^{\text{mix}}(u_1, u_2) &= \sum_{i=1}^{2} w_i C_i(u_1, u_2) \\ &= w_1 C_1(u_1, u_2) + w_2 C_2(u_1, u_2) \\ &= w_1 C_{\theta_1}^{\text{Frank}}(u_1, u_2) + w_2 C_{\theta_2}^{\text{Gumbel}}(u_1, u_2) \end{aligned}$$

Since $\sum_{i=1}^{m} = 1$, we have $w_1 + w_2 = 1 \implies w_2 = 1 - w_1$. This leads to

$$\begin{aligned} C_{FG}^{\text{mix}}(u_1, u_2) &= w C_{\theta_1}^{\text{Frank}}(u_1, u_2) + (1 - w) C_{\theta_2}^{\text{Gumbel}}(u_1, u_2) \\ C_{FG}^{\text{mix}}(u_1, u_2) &= w \left[-\frac{1}{\theta_1} \ln \left(1 + \frac{(e^{-\theta_1 u_1} - 1)(e^{-\theta_1 u_2} - 1)}{(e^{-\theta_1} - 1)} \right) \right] + \\ & \quad (1 - w) \left[e^{\left(-\left[(-\ln u_1)^{\theta_2} + (-\ln u_2)^{\theta_2} \right]^{\frac{1}{\theta_2}} \right)} \right] \end{aligned}$$

Table 7 shows the log-likelihood, AIC and BIC of the mixture of copula for GHI against temperature. The top panel of Figure 9 shows the range of bivariate behaviour represented by a Frank-Gumbel copula. As can be observed from the figures, the estimated Frank-Gumbel copula for GHI against temperature is characterised by lower and upper tails dependence.

Table 7. Frank-Gumbel mixture (GHI, temperature).

Parameter	Estimate	Copula	Std. Error
θ_1	4.0556	Frank	0.055
θ_2	1.5726	Gumbel	0.118
w_1	0.9513	Frank	0.243
w_2	0.0487	Gumbel	N/A
AIC	−10,168.58		
BIC	−10,135.71		
Log-likelihood	5088.29		
λ^U	0.2087		
λ^L	0		

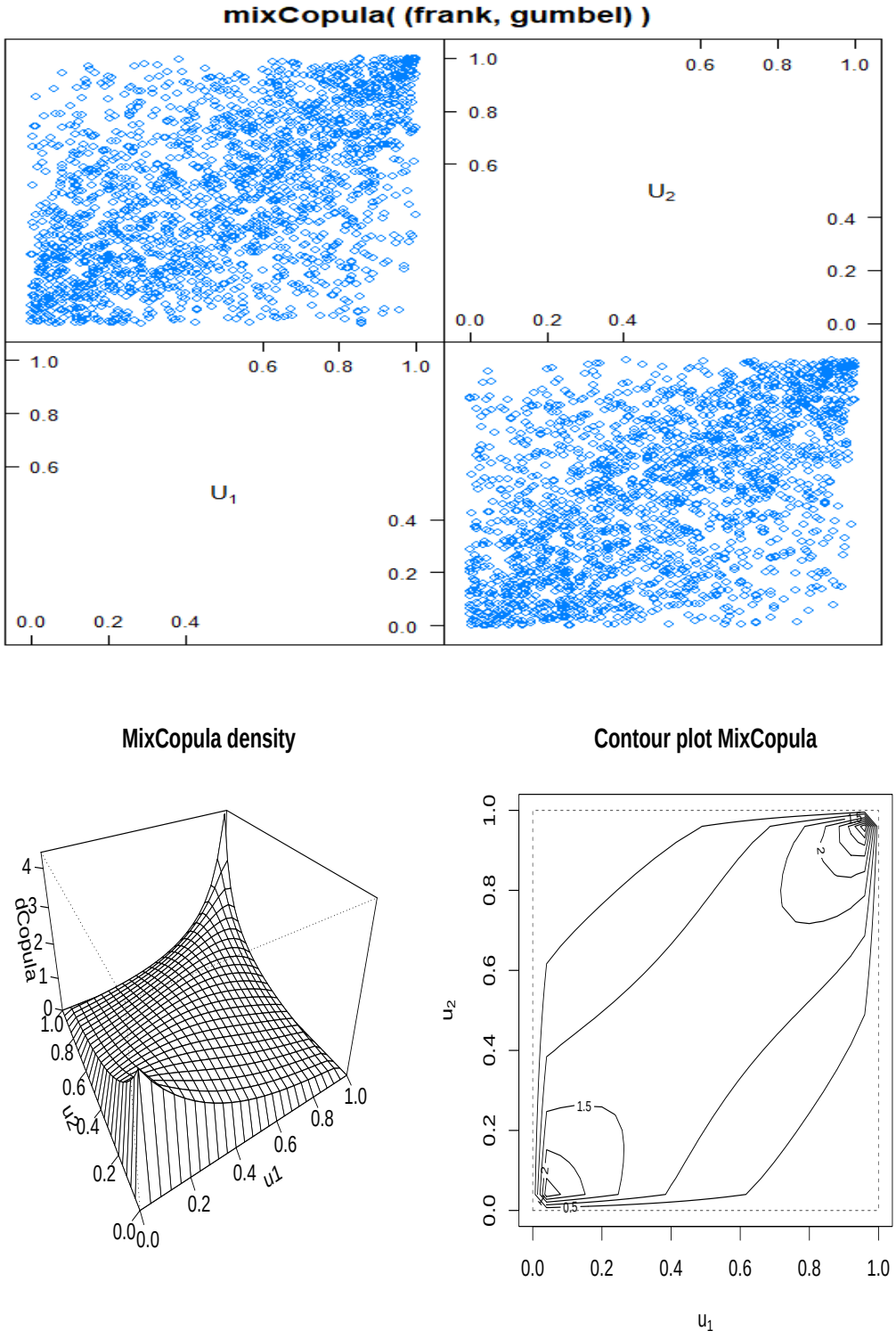

Figure 9. Top panel: Simulated standard uniform random variables under a MixCopula for GHI against temp. **Bottom panel:** Density and Contour plots of the joint distribution for the MixCopula of GHI against temp.

4. Discussion

This study was conducted on one radiometric station in South Africa using data for the period 16 November 2015 to 16 November 2021 to explore the extreme dependence of GHI on temperature and RH. MARS models were used to estimate the influence of two weather variables, temperature and relative humidity, respectively, on GHI. A plot of how the GHI output relates to temperature with the best line estimated by the MARS model is found in Figure 2 (top panel). It is shown that when the temperature increased between 0 °C and 19 °C, the GHI increased slightly and when the temperature increased between 19 °C and 30 °C, the GHI increased significantly. Again, when the temperature increased between 30 °C and 44 °C, the GHI increased slightly and this means that the relationship between temperature and GHI is directly proportional. Figure 2 (bottom panel) showed a plot of how the GHI output relates to RH with the best line estimated by the MARS model. It is shown that when RH increased between 0% and 48%, the GHI decreased slightly and when the RH increased between 48% and 84%, the GHI decreased significantly. Again, when RH increased between 84% and 100%, the GHI decreased slightly, which means that the relationship between RH and GHI is inversely proportional. This study examined the effect of marginal temperature increases above 30 °C on GHI. When $T_t > 30$ °C, we used

$$\hat{\text{GHI}} = 420 + 24 * \max(0, T_t - 19) \tag{24}$$

As the temperature increases from 30 to 31 °C, the marginal increase in GHI is 24 W/m^2, leading to 420 + 24 W/m^2, giving us a total of 444 W/m^2. For RH, we are interested in the effect of a marginal increase in RH above 84% on GHI. When $\text{RH}_t > 84\%$, we use

$$\hat{\text{GHI}} = 540 - 12 * \max(0, \text{RH}_t - 48) \tag{25}$$

As the RH increases from 84 to 85%, the marginal increase in GHI is –12 W/m^2, leading to 540–12 W/m^2, giving us a total of 528 W/m^2. This implies that when RH increases, the GHI decreases. Estimated quantiles at various tail probabilities and marginal increases in GHI are given in Table 4a,b for GHI against temperature and GHI against RH, respectively. The marginal increase in GHI converges to 0.12 W/m^2 when the temperature over the sampling period from 16 November 2015 to 16 November 2021 converges to 44.26 °C. As RH converges to 103.26%, the marginal increase of GHI converges to –0.1 W/m^2. In Section 3.2.4, the exploratory data analysis using the MCS plots was undertaken before bivariate conditional modelling of the dependence structure. The conditional bivariate extreme value modelling results are summarised in Table 5. The diagnostic plots for conditioning GHI on temperature and RH are presented in Figure 7. The dependence structure of GHI against temperature and RH was examined using the Archimedean copula functions such as Clayton, Frank, and Gumbel. The Frank copula for GHI against temperature better fits the data based on log-likelihood, AIC, and BIC since it has the highest log-likelihood and lowest AIC and BIC values. For GHI against RH, only the Frank copula adequately fits the data. The contour plots of the Archimedean copula functions were presented in Figure 8.

To our knowledge, no work has been done using conditional multivariate extreme value modelling of the extremal dependence modelling of GHI with the temperature and GHI with relative humidity. However, the use of copula models is discussed in the literature. From the study done by [17] the Gaussian copula, which is in the elliptical family, was found to be the best fitting to the clearness index and solar radiation data. The Clayton copula, which belongs to the Archimedean family, yielded the best performance based on the work done by [19] using the mean monthly solar radiation and sunshine duration hours data. Based on our studies, the Frank copula was the best fitting on GHI and temperature data, including the GHI and relative humidity data. The extremal dependence modelling from this study will help the decision-makers and planners in the energy sector plan the effects of extreme temperature and RH on GHI outputs.

5. Conclusions

This study presented an extremal dependence modelling of GHI with temperature and RH at one radiometric station using South African data from 16 November 2015 to 16 November 2021. In comparison, some studies have been conducted on the modelling of GHI, as well as a few studies on modelling GHI in South Africa (see [5,6]), no evidence of studies have been conducted on modelling extremal dependence of GHI with temperature and RH using the multivariate adaptive regression splines (MARS), extreme value theory and copula models. This is the gap this study bridged by modelling the effect of temperature and RH on GHI and the extremal dependence of GHI on temperature and RH. The results from the MARS models revealed that the relationship between GHI and temperature is directly proportional, whereas the relationship between GHI and RH is inversely proportional. The marginal increase at different quantiles also confirmed that when the temperature increases, the GHI also increases and when the RH increases, the GHI decreases. The conditional multivariate extreme value theory was used in modelling the dependence features on GHI with temperature and RH. Temperature and RH marginal diagnostic plots are linear, indicating that the parameterised tail fraction is appropriate for the data. In MCS plots, temperature and GHI are weakly correlated, but RH and GHI are negatively correlated. Conditioning on GHI helps to understand the significant negative extremal dependence of temperature and RH on large values of GHI. Since temperature is a major driver of GHI, extreme high temperature and RH implies some dependence on GHI. One of our findings is that the dependence structure between GHI and variable temperature and RH is asymmetric. Furthermore, the Frank copula is the best fitting model for variable temperature and RH, implying the presence of extreme co-movements. The results from this study could be helpful to decision-makers in power utility companies that face uncertainty in GHI power production due to extreme temperatures and RH.

Author Contributions: Conceptualization, T.R. and C.S.; methodology, T.R. and C.S.; software, T.R.; validation, T.R. and C.S.; formal analysis, T.R.; investigation, T.R.; data curation, T.R. and C.S.; writing—original draft preparation, T.R.; writing—review and editing, T.R., C.S. and L.J.; visualisation, T.R. and C.S.; supervision, C.S. and L.J.; project administration, C.S. and L.J.; funding acquisition, T.R. and C.S. All authors have read and agreed to the published version of the manuscript.

Funding: The authors acknowledge the DSI—CSIR Inter bursary Support (IBS) Programme for financial support.

Institutional Review Board Statement: Not applicable.

Informed Consent Statement: Not applicable.

Data Availability Statement: The data used in this study are from Southern African Universities Radiometric Network (SAURAN), website (https://sauran.ac.za/, accessed on 17 November 2021).

Acknowledgments: The authors acknowledge the DSI—CSIR Inter bursary Support (IBS) Programme for financial support and to both SAURAN, Southern African Universities Radiometric Network and the South African Weather Services for providing the data.

Conflicts of Interest: The authors declare no conflict of interest.

Abbreviations

The following abbreviations are used in this manuscript:

GHI	Global horizontal irradiance
RH	Relative humidity
PV	Photovoltaic
KNN	K–nearest neighbour
SVM	Support vector machine
MARS	Multivariate Adaptive Regression Spline
GCV	Generalised cross–validation

CEM	Conditional extremes model
GPD	Generalised Pareto distribution
EVT	Extreme value theory
AIC	Akaike information criterion
BIC	Bayesian information criterion
SAURAN	Southern African Universities Radiometric Network
MDPI	Multidisciplinary Digital Publishing Institute

Appendix A

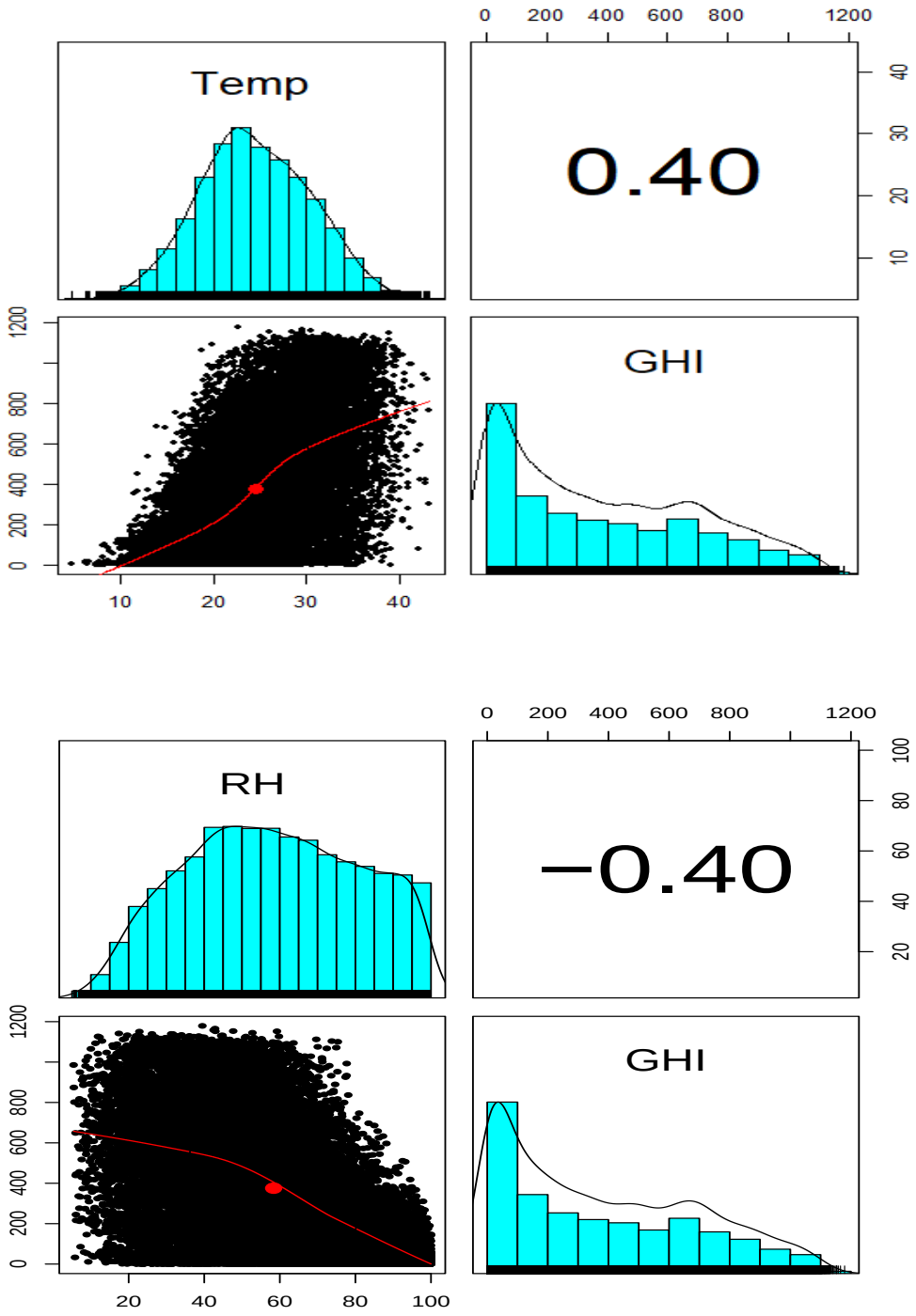

Figure A1. Top panel: Pairs panel GHI against temperature using Kendall method. **bottom panel:** Pairs panel GHI and relative humidity.

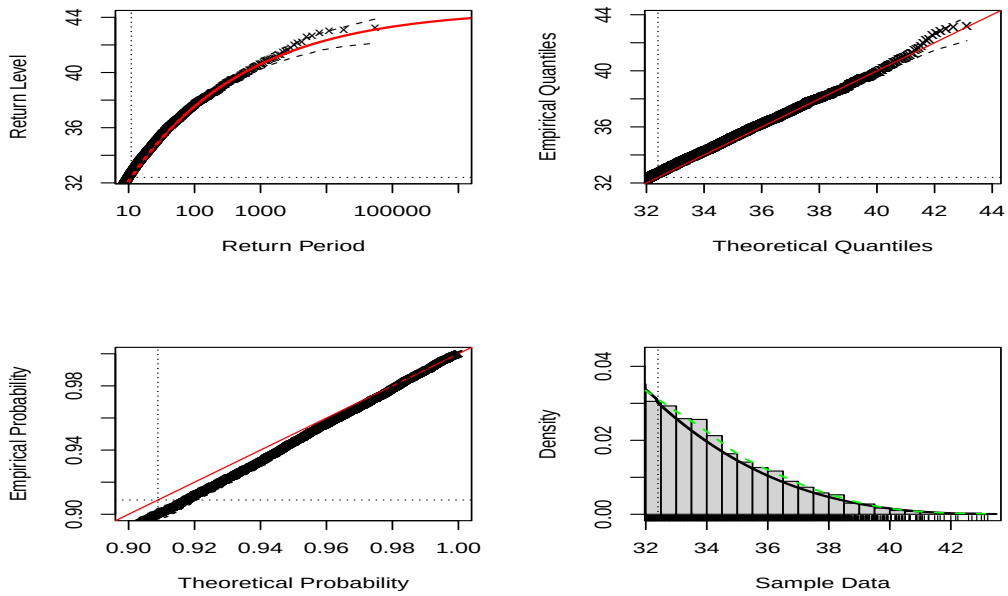

Figure A2. Diagnostic plots for fitted Bulk model of Temperature.

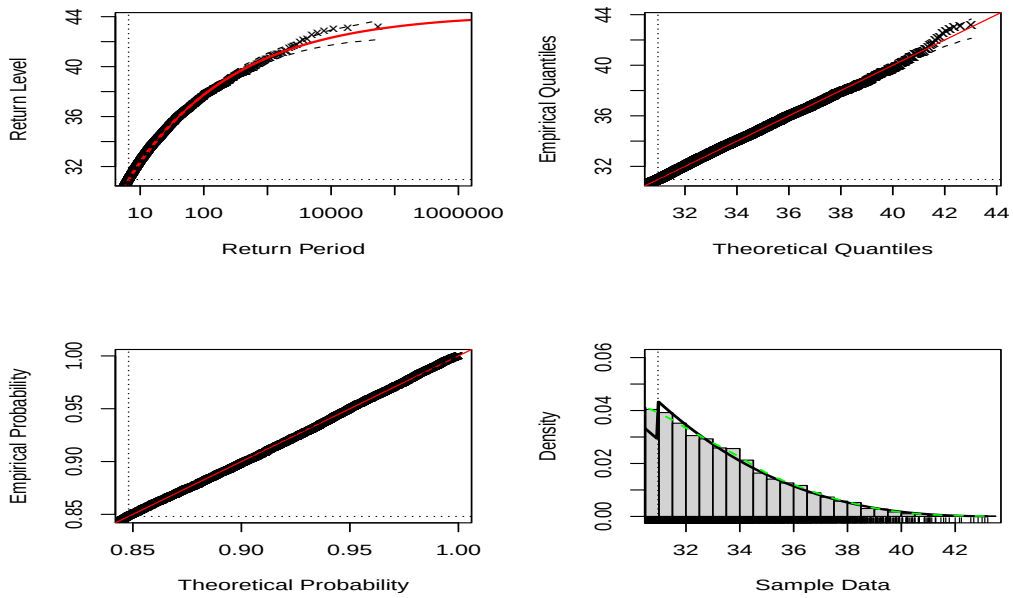

Figure A3. Diagnostic plots for fitted Parameterised tail fraction of Temperature.

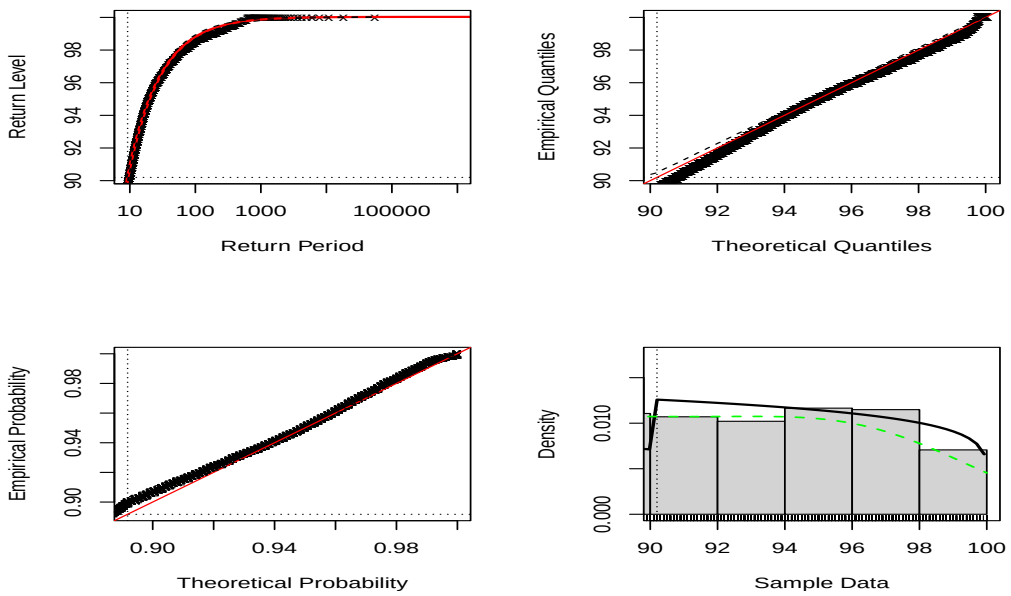

Figure A4. Diagnostic plots for fitted bulk model of relative humidity.

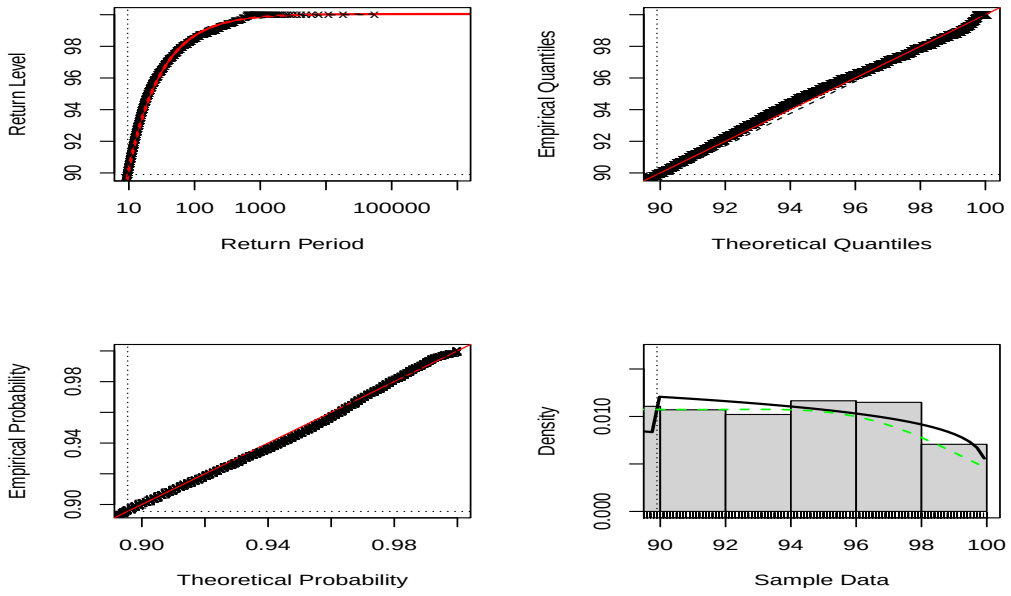

Figure A5. Diagnostic plots for fitted parameterised tail fraction of relative humidity.

References

1. Alresheedi, A.A.; Al-Hagerty, M.A. Forecasting the Global Horizontal Irradiance Based on Boruta Algorithm and Artificial Neural Networks using a Lower Cost. *(IJACSA) Int. J. Adv. Comput. Sci. Appl.* **2020**, 11, 79–92. [CrossRef]
2. Heinemann, D.; Lorenz, E.; Girodo, M. Forecasting of solar radiation. In *Solar Energy Resource Management for Electricity Generation from Local Level to Global Scale*; Nova Science Publishers: New York, NY, USA, 2006; pp. 83–94. Available online: https://citeseerx.ist.psu.edu/viewdoc/download?doi=10.1.1.526.2530&rep=rep1&type=pdf (accessed on 5 November 2021).
3. Gao, B.; Huang, X.; Shi, J.; Tai, Y.; Zhang, J. Hourly forecasting of solar irradiance based on CEEMDAN and multi-strategy CNN-LSTM neural networks. *Renew. Energy* **2020**, 162, 1665–1683. [CrossRef]
4. Mishra, M.; Dash, P.B.; Nayak, J.; Naik, B.; Swain, S.K. Deep learning and wavelet transform integrated approach for short-term solar PV power prediction. *Measurement* **2020**, *166*, 108250. [CrossRef]
5. Chandiwana, E.; Sigauke, C.; Bere, A. Twenty-Four-Hour Ahead Probabilistic Global Horizontal Irradiance Forecasting Using Gaussian Process Regression. *Algorithms* **2021**, 14, 177. [CrossRef]

6. Mutavhatsindi, T.; Sigauke, C.; Mbuvha, R. Forecasting Hourly Global Horizontal Solar Irradiance in South Africa Using Machine Learning Models. *IEEE Access* **2020**, *8*, 198872–198885. [CrossRef]
7. Diagne, M.; David, M.; Lauret, P.; Boland, J.; Schmutz, N. Review of solar irradiance forecasting methods and a proposition for small-scale insular grids. *Renew. Sustain. Energy Rev.* **2013**, *27*, 65–76. [CrossRef]
8. Li, Y.; He, Y.; Su, Y.; Shu, L. Forecasting the daily power output of a grid-connected photovoltaic system based on multivariate adaptive regression splines. *Appl. Energy* **2016**, *180*, 392–401. [CrossRef]
9. Li, D.H.; Chen, W.; Li, S.; Lou, S. Estimation of hourly global solar radiation using Multivariate Adaptive Regression Spline (MARS)—A case study of Hong Kong. *Energy* **2019**, *186*, 115857. [CrossRef]
10. Sigauke, C.; Chikobvu, D. Daily peak electricity load forecasting in South Africa using a multivariate nonparametric regression approach. *ORiON* **2010**, *26*, 317–403. [CrossRef]
11. Heffernan, J.E.; Tawn, J.A. A conditional approach for multivariate extreme values (with discussion). *J. R. Stat. Soc. Ser. B (Stat. Methodol.)* **2004**, *66*, 497–546. [CrossRef]
12. Keef, C.; Papastathopoulos, I.; Tawn, J.A. Estimation of the conditional distribution of a multivariate variable given that one of its components is large: Additional constraints for the Heffernan and Tawn model. *J. Multivar. Anal.* **2013**, *115*, 396–404. [CrossRef]
13. Tilloy, A.; Malamud, B.D.; Winter, H.; Joly-Laugel, A. Evaluating the efficacy of bivariate extreme modelling approaches for multi-hazard scenarios. *Nat. Hazards Earth Syst. Sci.* **2020**, *20*, 2091–2117. [CrossRef]
14. Maposa, D.; Seimela, A.M.; Sigauke, C.; Cochran, J.J. Modelling temperature extremes in the Limpopo province: Bivariate time-varying threshold excess approach. *Nat. Hazards* **2021**, *107*, 2227–2246. [CrossRef]
15. Nemukula, M.M.; Sigauke, C.; Maposa, D. Bivariate threshold excess models with application to extreme high temperatures in Limpopo province of South Africa. In Proceedings of the 60th Annual Conference of the South African Statistical Association for 2018, Roodepoort, South Africa, 26–29 November 2018; pp. 33–40. Available online: https://hdl.handle.net/10520/EJC-1298c323dd (accessed on 17 November 2021).
16. Nelsen, R.B. *An Introduction to Copulas*, 2nd ed.; Springer Series in Statistics Springer; Springer: Berlin/Heidelberg, Germany, 2006.
17. Yet, Z.R.; Masseran, N. Modeling dependence of solar radiation and sky clearness index using a bivariate copula. *Meteorol. Atmos. Phys.* **2021**, *133*, 1495–1504. [CrossRef]
18. Munkhammar, J.; Widén, J. Correlation modeling of instantaneous solar irradiance with applications to solar engineering. *Sol. Energy* **2016**, *133*, 14–23. [CrossRef]
19. Bazrafshan, J., Heidari, N., Moradi, I., Aghashariatmadary, Z. Simultaneous Stochastic Simulation of Monthly Mean Daily Global Solar Radiation and Sunshine Duration Hours Using Copulas. *J. Hydrol. Eng.* **2015**, *20*, 1–11. [CrossRef]
20. Prieto, J.I.; Martínez-García, J.C.; García, D. Correlation between global solar irradiation and air temperature in Asturias, Spain *Sol. Energy* **2009**, *83*, 1076–1085. [CrossRef]
21. Friedman, J. Multivariate adaptive regression splines. *Ann. Stat.* **1991**, *19*, 1–141. Available online: http://www.jstor.org/stable/2241837 (accessed on 29 November 2021). [CrossRef]
22. Craven, P.; Wahba, G. Smoothing Noisy Data with Spline Functions. Estimating the Correct Degree of Smoothing by the Method of Generalised Cross-Validation. *Numer. Math.* **1979**, *31*, 317–403. [CrossRef]
23. Coles S. *An Introduction to Statistical Modelling of Extreme Values*; Springer: London, UK, 2001.
24. Scarrott, C. and MacDonald, A. A review of extreme value threshold estimation and uncertainty quantification. *REVSTAT—Stat. J.* **2012**, *10*, 33–60. [CrossRef]
25. Hu, Y. Extreme Value Mixture Modelling with Simulation Study and Applications in Finance and Insurance. Master's Thesis, University of Cantebury, Christchurch, New Zealand, 2013. [CrossRef]
26. Naifar, N. Modelling dependence structure with Archimedean copulas and applications to the iTraxx CDS index. *J. Comput. Appl. Math.* **2011**, *235*, 2459–2466. [CrossRef]
27. Mupondo, N.C.; Jones, C.B.; Sigauke, C. The Volatility Spillovers between Zimbabwe, The United States of America, South Africa, Botswana and China: Copula GARCH Model. *J. Risk Financ. Stud.* **2021**, *2*, 105–139. Available online: https://arfjournals.com/image/71326_6_ndava_constantine.pdf (accessed on 28 December 2021).
28. Corbella, S.; Stretch, D.D. Simulating a multivariate sea storm using Archimedean copulas. *Coast. Eng.* **2013**, *76*, 68–78. [CrossRef]
29. Clayton, D.G. A model for association in bivariate life tables and its application in epidemiological studies of familial tendency in chronic disease incidence. *Biometrika* **1978**, *65*, 141–151. [CrossRef]
30. Frank, M.J. On the simultaneous associativity of F(x,y) and x + y—F(x,y). *Aequationes Math.* **1979**, *19*, 194–226. [CrossRef]
31. Gumbel, E.J. Distributions des valeurs extremes en plusiers dimensions. *Publ. Inst. Statist. Univ. Paris* **1960**, *9*, 171–173.
32. Wood, S.N. *Generalized Additive Models: An Introduction with R*; CRC Press: Boca Raton, FL, USA, 2017.
33. Milborrow, S. Earth: Multivariate Adaptive Regression Splines, R Package Version 4.6.3. 2018. Available online: https://cran.r-project.org/web/packages/earth/index.html (accessed on 23 October 2021).
34. Hu, Y.; Scarrott, C.J. Evmix: An R Package for Extreme Value Mixture Modeling, Threshold Estimation and Boundary Corrected Kernel Density Estimation. 2018. Available online: https://cran.r-project.org/web/packages/evmix/index.html (accessed on 6 January 2022).